A5 ANORTHITE-MELT PARTITIONING OVER A RANGE (40-60 WT.%) OF MELT SILICA CONTENT

A5.1 Composition Selection of Variable SiO_2 Melts (CMAS1 Suite) for Partitioning Experiments

A study of anorthite-melt partitioning with six melt compositions (CMAS1) varying in SiO_2 content was attempted, since magma in natural systems generally evolves from mafic to more felsic compositions. However, this section demonstrates that melt influence on partitioning could not be isolated in these experiments due to resulting covariance in crystal and melt chemistry. As discussed in Section 2.2.1, anorthite crystals synthesized at low pressure can incorporate up to 15 wt. % excess silica component into their structures (Bruno and Facchinelli, 1974) depending on the silica content of the coexisting melt and crystal growth rate (Beaty and Albee, 1980). This proved true for the anorthites grown from the CMAS1 compositions.

Figure A5.1 shows the locations of the starting compositions for the six CMAS1 melts projected onto the CAS ternary. Although these compositions all contain ~1 wt. % MgO, a CAS diagram is a reasonably accurate simplification of the composition space. Materials were prepared according to the procedures outlined in Section 2.2.4 except that the doping concentrations were 1500 ppm Ba and 1000 ppm Sr. Isothermal experiments were conducted to constrain the liquidi and confirmed all were at or near the 1400 °C anorthite liquidus as predicted by the Berman (1983) CMAS thermodynamic melt model. Liquidus temperatures for the six CMAS1 compositions are displayed in Table A5.1.

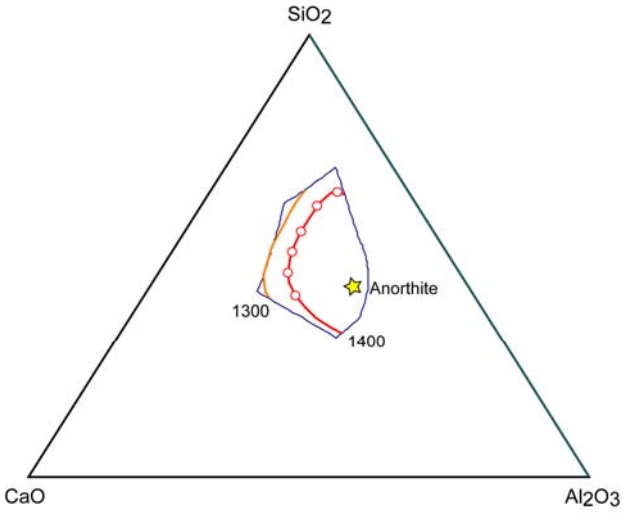

Figure A5.1. CMAS1 melt compositions shown in red circles on the 1400 °C liquidus isotherm within the anorthite stability field (outlined in blue) projected onto the CAS ternary (wt. %). The 1300 °C liquidus isotherm is shown in orange.

A5.2 CMAS1 Anorthite and Melt Composition Data and Evidence of SiO_2 and Na_2O Solid Solution

Compositions of phases present in the CMAS1 experimental charges (run conditions listed in Table A6.1) were measured with the Caltech 733 electron microprobe using analytical conditions and standards described in Section A1.3 and Section 2.2.4, respectively. Table A5.1 lists the starting material contents, which, for the purposes of calculating partition coefficients for these experiments, are assumed to be the melt compositions from which the centers of anorthite crystals initially grew.

Anorthite and coexisting glass contents of select dynamic crystallization experiments of each melt composition are listed in Table A5.2 and Table A5.3. The dependence of excess silica component incorporation into the anorthite structure on melt SiO_2 content is shown in Figure A5.2. When melt compositions contain less than 50

wt. % SiO_2 the excess [ ]Si_4O_8 component varies little within analytical uncertainty, but at higher melt silica contents silica solid solution increases significantly.

Table A5.1. Initial melt compositions (wt. %) determined by EMP analysis of glass points. Uncertainty reported as standard error of the mean in parentheses and applies to the last digit shown. Liquidus uncertainties are ± 5 °C.

	1-1-1 n = 5	1-2-1 n = 5	1-3-1 n = 5	1-4-1 n = 5	1-5-1 n = 5	1-6-1 n = 5
Liquidus (°C)	1393	1395	1407	1407	1407	1417
SiO_2	39.73 (6)	44.5 (1)	49.72 (6)	53.59 (7)	59.2 (2)	62.1 (3)
Al_2O_3	27.16 (9)	23.39 (9)	21.12 (4)	20.96 (4)	21.1 (1)	22.6 (1)
MgO	0.94 (1)	0.92 (1)	0.92 (1)	0.94 (1)	0.92 (1)	0.96 (1)
CaO	30.66 (5)	29.76 (5)	26.26 (5)	23.06 (4)	17.12 (6)	12.63 (7)
SrO	0.12 (1)	0.14 (1)	0.11 (3)	0.12 (1)	0.08 (2)	0.12 (1)
BaO	0.19 (2)	0.17 (2)	0.19 (3)	0.16 (1)	0.21 (3)	0.22 (2)
Na_2O	0.96 (1)	1.06 (1)	1.25 (3)	1.38 (1)	1.72 (1)	1.64 (2)
	99.81	99.99	99.59	102.2	100.33	100.24

Table A5.2. CMAS1 anorthite compositions (wt. %) determined by EMP analyses of random points in crystal centers. 1 σ error parentheses apply to the last digit shown.

	1-1-2 n = 10 MgO, SrO, BaO: n = 30	1-2-2 n = 10 MgO, SrO, BaO: n = 30	1-3-9 n = 10 MgO, SrO, BaO: n = 30	1-4-11 n = 10 MgO, SrO, BaO: n = 30	1-5-9 n = 10 MgO, SrO, BaO: n = 30	1-6-8 n = 10 MgO, SrO, BaO: n = 30
SiO_2	42.8 (4)	43.4 (4)	44.7 (2)	45.6 (5)	47.1 (6)	48.2 (7)
Al_2O_3	36.5 (3)	36.3 (4)	35.3 (3)	34.8 (5)	33.0 (5)	33.1 (4)
MgO	0.009 (9)	0.019 (5)	0.083 (7)	0.088 (7)	0.08 (1)	0.058 (9)
CaO	20.3 (2)	20.14 (9)	19.4 (1)	18.89 (9)	18.4 (1)	18.1 (3)
SrO	0.11 (1)	0.114 (6)	0.118 (6)	0.100 (6)	0.101 (6)	0.107 (6)
BaO	0.04 (1)	0.03 (1)	0.027 (9)	0.020 (7)	0.015 (9)	0.016 (9)
Na_2O	0.03 (2)	0.19 (3)	0.46 (5)	0.51 (2)	0.50 (3)	0.43 (3)
	99.78	100.19	100.09	100.01	99.20	100.01

Table A5.3. CMAS1 glass compositions (wt. %) determined by EMP analysis of random points throughout the sample charge. 1 σ error parentheses apply to the last digit shown.

	1-1-2 n = 10	1-2-2 n = 10	1-3-9 n = 10	1-4-11 n = 10	1-5-9 n = 10	1-6-8 n = 10
SiO_2	38.2 (4.4)	44.7 (6)	51.0 (2)	55.3 (7)	62.0 (3)	66.0 (2.2)
Al_2O_3	25.1 (2.3)	18.9 (3)	18.3 (1)	18.6 (4)	18.4 (3)	19.6 (1.4)
MgO	1.23 (8)	1.25 (2)	1.12 (2)	1.13 (3)	1.12 (2)	1.4 (1)
CaO	34.8 (2.0)	34.1 (2)	28.6 (1)	24.08 (1)	17.3 (2)	11.4 (8)
SrO	0.11 (5)	0.12 (4)	0.12 (3)	0.13 (3)	0.13 (4)	0.12 (2)
BaO	0.24 (7)	0.21 (8)	0.19 (6)	0.20 (7)	0.19 (8)	0.33 (6)
Na_2O	0.25 (2)	0.34 (9)	0.43 (2)	0.48 (3)	0.53 (2)	0.63 (5)
	99.93	99.62	99.76	99.92	99.67	99.48

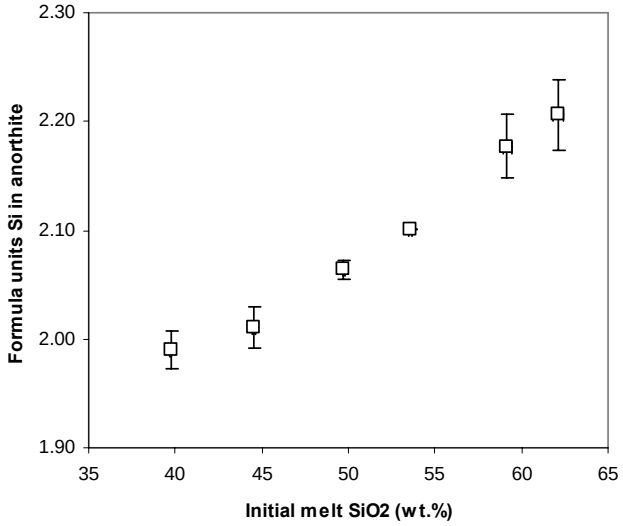

Figure A5.2. Incorporation of excess silica component [ ]Si_4O_8 into anorthite structure reported as increase in formula units of Si measured in CMAS1 suite anorthites as a function of initial melt SiO_2 content. Error bars represent 1σ uncertainty in anorthite composition analysis. Melt analysis error is within symbol size.

Although no Na_2O was included in the starting material, some run products of Pt wire experiments that remained in the furnace without any gas flow for durations longer than 15 minutes experienced over 1.5 wt. % sodium contamination (Figure A5.3). Since maintaining uniform crystal chemistry in anorthites from all six CMAS1 compositions

was necessary to isolate the effect of melt composition on partitioning, having varying levels of sodium contamination in the furnace proved problematic. Anorthite data in Table A5.2 indicate that the crystals on average contain between 0.2 % and 5 % of an albitic component. Neutralizing this effect by subjecting experimental charges for all six compositions to the same furnace conditions by running them concurrently was not an option, as the differences in liquidus temperatures for the starting materials was great enough to require slightly different controlled cooling programs in order to grow crystals. Use of Pt capsules and flows of various gases (Ar, CO, and compressed air) all reduced sodium contamination to within or just above EMP detection limits, though the anorthite and glass data for the CMAS1 compositions were all collected on samples run in stagnant air prior to this discovery. Subsequent experiments involving the CMAS2 and CMAS2b compositions all used some form of gas flow to minimize sodium partial pressure in the furnace during runs.

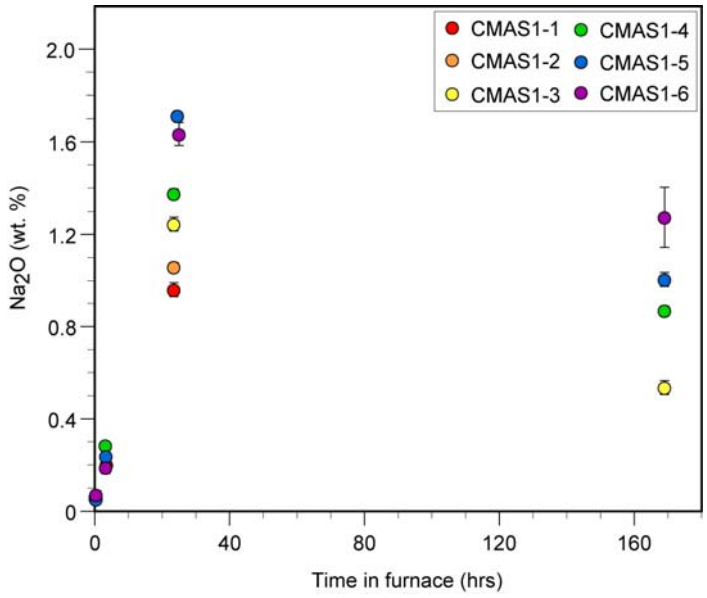

Figure A5.3. Glass Na_2O (wt. %) content change as a function of time in furnace.

Estimates of Mg distribution between IV- and VIII-fold coordinated sites in anorthite for partition coefficient modeling followed the method described in Section 2.3.3. Compositional data for CMAS1 are less precise than those of CMAS2b (chapter 2) due to use of a lower beam current during analysis and only collecting data points from crystal interiors, which may be more heterogeneous than crystal rims. Both these factors likely contribute to the large uncertainties shown in Figure A5.3. Although the equations relating Mg site occupancy to melt chemistry in Section 2.3.3 do not explicitly account for the presence of excess silica in the anorthite phase, the Berman (1983) melt model may be assumed to have incorporated the effects of this solid solution on activity coefficients because it was calibrated and tested using liquidus data from anorthite-melt experiments throughout the anorthite stability field, which includes high silica melts (>50 wt. % SiO_2). This study and others (e.g., Bruno and Facchinelli, 1974; Ito, 1976; Longhi and Hays, 1979; Murakami et al., 1992) have shown such melts produce anorthite with an excess silica component likely not recognized without careful quantitative compositional analysis of crystals larger than those generated in near-liquidus experiments. The $D^m MgO$-melt major activity product relationship used to predict $D^m{}_{MgVIII}$ in CMAS1 compositions is plotted in Figure A5.4.

CMAS1 anorthite-melt molar partition coefficients for major and trace elements are listed in Table A5.4. *D* values are calculated using the initial starting compositions of Table A5.1 and anorthite center point averages reported in Table A5.2. $D^m{}_{MgOVIII}$ and $D^m{}_{CaO}$ both increase as the melts become progressively siliceous, but the errors associated with the SrO partitioning data are too large to identify a similar trend for that element.

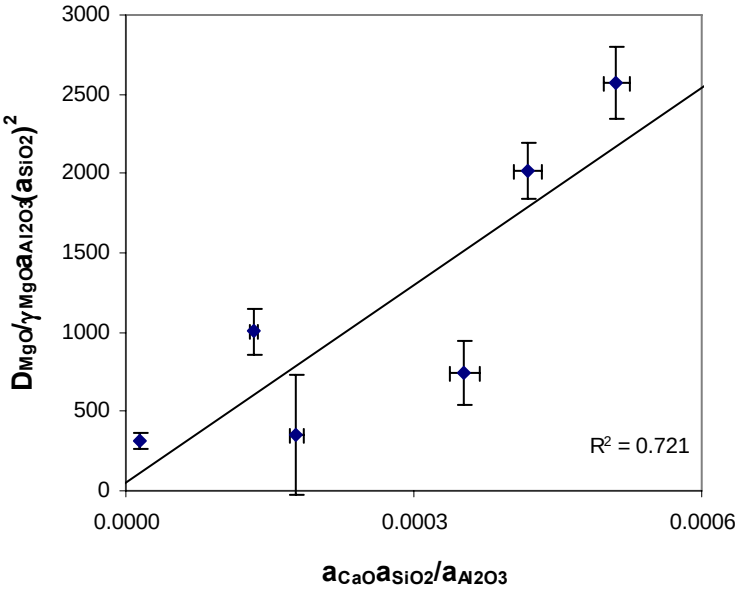

Figure A5.4. Relationship observed D^m_{MgO} and melt activity products (from Berman (1983) CMAS melt model) expected for Mg^{2+} partitioning onto IV- and VIII-fold coordination sites of anorthite crystal lattice. 1 σ error bars for activity products are propagations of activity uncertainties due to compositional uncertainty. No estimate is made of systematic errors inherent in the activity model.

Table A5.4. Anorthite/melt partitioning in CMAS1 compositions at ~1400 °C. $D^m_{MgOVIII}$ values are calculated following the method outlined in chapter 2, using the linear relationship between D^m_{MgO} and major element activity products to predict Mg site occupancy in anorthite. Uncertainties are propagations of the standard error of the mean and 1 σ analytical errors for the glass and anorthite phases, respectively, and are given in parentheses, referring to the final digit reported for each value.

	D^m_{SiO2}	D^m_{Al2O3}	D^m_{MgO}	$D^m_{MgOVIII}$	D^m_{CaO}	D^m_{SrO}	D^m_{BaO}
1-1-2	1.14 (1)	1.42 (1)	0.01 (1)	0.0015	0.700 (5)	0.97 (9)	0.22 (6)
1-2-2	1.04 (1)	1.66 (2)	0.022 (5)	0.0017	0.724 (3)	0.87 (7)	0.20 (7)
1-3-9	0.961 (4)	1.79 (2)	0.096 (8)	0.0021	0.792 (5)	1.2 (3)	0.15 (6)
1-4-11	0.914 (1)	1.78 (1)	0.101 (8)	0.0029	0.881 (1)	0.89 (9)	0.13 (5)
1-5-9	0.85 (1)	1.68 (3)	0.09 (1)	0.0053	1.153 (9)	1.4 (3)	0.08 (5)
1-6-8	0.82 (1)	1.54 (2)	0.06 (1)	0.0115	1.51 (2)	0.9 (1)	0.08 (4)

Interestingly, D^m_{BaO} exhibits partitioning behavior opposite that of $D^m_{MgOVIII}$ and D^m_{CaO}. It is unclear whether this difference results from the structural variations in

anorthite due to excess silica that promote incorporation of Ba or possible kinetic effects of crystal growth from increasingly viscous melts that could allow large Ba melt concentration gradients to develop around the crystals. Anorthite clearly grows differently from highly siliceous melts than in more mafic compositions under the same thermal regime, as indicated by the visible changes in crystal morphology shown in Figure A4.5, where crystal of experiment 1-6-8 (c) are less well formed than in 1-1-2 (a) or 1-3-9 (b).

A5.3 Lattice Strain Parameterizations of CMAS1 Divalent Element Partitioning Data

Lattice strain parameters were calculated from CMAS1 divalent element partitioning data according to the methods described in Section A4.1 and are given in Table A5.5. Goodness of fit, χ^2, is relatively low compared to values calculated for parameterizations in chapter 2 because the analytical precision of the CMAS1 data is much lower. If changes in crystal structure are dominating the Ba partitioning behavior observed and the activity coefficient of Ba in the solid varies little, the strain parameter (E) calculated from the Ba data suggests that the anorthite structure around the large M site may becomes more rigid as silica content increases in the anorthite and/or melt. Parameterizations of the ideal ionic radius of the crystal site (r_o) for these compositions show no systematic variations. D_o, however, increases with increasing melt silica content in a manner primarily dictated by the partitioning systematics of $D^m_{MgOVIII}$ and D^m_{CaO}. Parameterized curves (D vs. ionic radius) for CMAS1 are plotted in Figure A5.5 with the partitioning data of Table A5.5.

Table A5.5. Lattice strain model parameterization after Blundy and Wood (1994) for CMAS1 divalent element (Mg, Ca, Sr, Ba) partitioning data. Parameterization uses calculated $D^{m}MgO_{VIII}$ shown in Table A5.4 and assumes an uncertainty of 10% relative for those values. $\chi^2 = [(\ln D^{data} - \ln D^{model})/\ln\sigma^{data}]^2$ for each parameterization.

	D_o	E (GPa)	r_o (Å)	χ^2
1-1-2	1.10	170 (20)	1.213 (2)	14.2
1-2-2	1.07	180 (20)	1.203 (1)	14.5
1-3-9	1.36	210 (20)	1.212 (3)	3.7
1-4-11	1.24	210 (20)	1.192 (1)	8.0
1-5-9	1.79	220 (20)	1.200 (4)	0.3
1-6-8	1.79	240 (20)	1.169 (2)	2.4

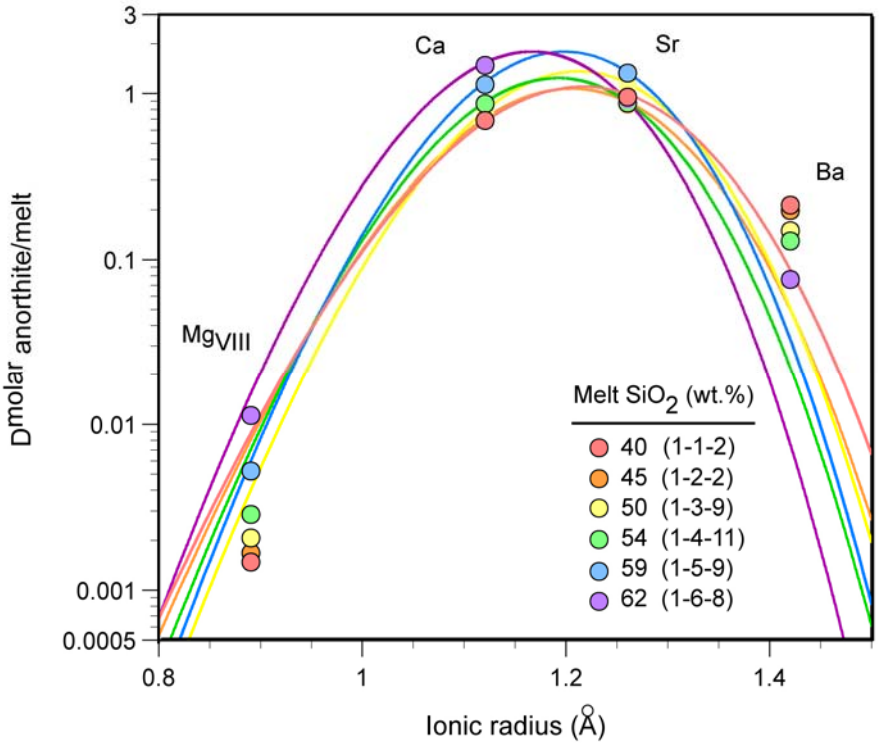

Figure A5.5. Onuma diagram of lattice strain parameterizations listed in Table A5.5 for divalent element (Mg, Ca, Sr, Ba) partitioning data of the CMAS1 melt compositions. Error bars on partition coefficients are omitted for clarity.